α-decay and fusion phenomena in heavy ion collisions using nucleon-nucleon interactions derived from relativistic mean-field theory

BirBikram Singh,* B. B. Sahu, and S. K. Patra†
Institute of Physics, Sachivalaya Marg, Bhubaneswar 751005, India
(Received 1 March 2011; revised manuscript received 25 April 2011; published 2 June 2011)

Nucleus-nucleus potentials are determined in the framework of the double-folding model for a new microscopic nucleon-nucleon (NN) interaction relativistic mean field-3-Yukawa (R3Y) derived from the popular relativistic mean-field theory Lagrangian, and the results are compared for the use of Michigan-3-Yukawa (M3Y) effective NN interactions. The double-folding potentials so obtained are further taken up in the context of the preformed cluster model (PCM) of Gupta and collaborators and the barrier penetration model to study respectively the ground-state (g.s.) α-decay and low-energy fusion reactions. In this paper, using PCM, we deduce empirically the α preformation probability ${P_0}^{\alpha(\mathrm{emp})}$ from experimental data on a few g.s. α decays in the trans-lead region. For fusion reactions, two projectile-target systems $^{12}\mathrm{C}+{}^{208}\mathrm{Pb}$ and $^{16}\mathrm{O}+{}^{208}\mathrm{Pb}$ are selected for calculating the barrier energies as well positions, fusion cross sections (σ_{fus}), and fusion barrier distribution [$D(E_{\mathrm{c.m.}})$]. The barrier energies and positions change for the R3Y NN interactions in comparison with those of the M3Y NN interactions. We find that in the α-decay studies the values of ${P_0}^{\alpha(\mathrm{emp})}$(R3Y) are similar to those of ${P_0}^{\alpha(\mathrm{emp})}$(M3Y). Further, both NN interactions give similar σ_{fus} values using the Wong formula specifically when the R3Y NN interaction calculated σ_{fus} values are reduced by 1.5 times, and the results are in agreement with the experimental data for both the systems, especially for the higher energies. Results for $D(E_{\mathrm{c.m.}})$ are also quite similar for both choices of NN interaction.

DOI: 10.1103/PhysRevC.83.064601 PACS number(s): 23.70.+j, 52.58.Hm, 25.70.−z

I. INTRODUCTION

The ground-state (g.s.) α-decay and heavy ion fusion reactions are quite important to investigate a number of nuclear phenomena; the nucleon-nucleon (NN) interaction is one of them. The nucleus-nucleus potentials in the study of α-decay and fusion reactions may be obtained by using effective NN interactions, which are remarkably related in the double-folding model (DFM) [1]. It is obtained in DFM by using an effective NN interaction, like the phenomenological Michigan-3-Yukawa (M3Y) plus a zero-range pseudopotential or a density-dependent M3Y, folded over the matter densities of the projectile-target nuclei. Recently, we and collaborators have introduced a microscopic NN interaction relativistic mean field-3-Yukawa (R3Y) [2] from the linear relativistic mean-field theory (RMFT) [3–6] Lagrangian rather than a simple phenomenological prescription. Moreover, we demonstrated its application [2] to various nuclear systems for evaluating some of the physical observables in the phenomenon of exotic cluster radioactivity (CR) by folding it with the RMFT densities of cluster and daughter nuclei to obtain the nucleus-nucleus potential, and results obtained were found to be comparable with the successfully used M3Y effective NN interactions.

In the present work, we employ it to investigate the g.s. α decay of few nuclei in trans-lead region and low-energy heavy ion fusion reactions using two projectile-target systems, $^{12}\mathrm{C}+{}^{208}\mathrm{Pb}$ and $^{16}\mathrm{O}+{}^{208}\mathrm{Pb}$, which have been studied experimentally quite extensively [7,8] and compare our results with that of the use of the phenomenological M3Y effective NN interaction, also. Our methodology for the study is to use the linear RMFT-HS and the barrier penetration model (BPM) described briefly in the following. The nuclear matter densities ρ_1 and ρ_2 are calculated by using the linear RMFT-HS formalism for spherical nuclei. Then, the nucleus-nucleus potential is obtained by using the well-known double-folding procedure to the M3Y [1] (or R3Y, proposed by us and collaborators in a very recent study [2]) interaction, supplemented by a zero-range pseudopotential representing the single-nucleon exchange effects (EX). The Coulomb potential V_C [$V_C(R) = Z_p Z_t e^2/R$] is calculated to obtain the total interaction potential $V(R) = V_n(R) + V_C(R)$ between the nuclei. Further, within the preformed cluster model (PCM) of Gupta and collaborators [9,10], we deduce empirically the α preformation probability ${P_0}^{\alpha(\mathrm{emp})}$ from experimental data on a few g.s. α decays in the trans-lead region. Also, within the BPM we obtain total fusion cross sections (σ_{fus}) using the well-known Wong formula [11].

II. FORMALISM

In the RMFT model [3–6], an effective Lagrangian is taken to describe the nucleons interacting through the effective meson and electromagnetic (e.m.) fields. The equations of motion are obtained using the Euler-Lagrange variational principle. A set of coupled equations results from replacing the field operators by their expectation values. A set of Klein-Gordon-type equations are yielded for mesons and photons with sources having nucleonic currents and densities, and the Dirac equation describing the nucleon dynamics is yielded with potential terms having the e.m. and meson fields. This set of RMFT-generated equations then is solved self-consistently to obtain the matter (neutron + proton) densities for the projectile and target nuclei to treat them further for obtaining the nuclear interaction potential between them.

*singh@iopb.res.in
†patra@iopb.res.in

The linear, relativistic mean-field Lagrangian density for a nucleon-meson many-body system [3–6] is

$$\begin{aligned} L = {} & \overline{\psi_i}\{i\gamma^\mu\partial_\mu - M\}\psi_i + \tfrac{1}{2}\partial^\mu\sigma\,\partial_\mu\sigma - \tfrac{1}{2}m_\sigma^2\sigma^2 \\ & - g_\sigma\overline{\psi_i}\psi_i\sigma - \tfrac{1}{4}\Omega^{\mu\nu}\Omega_{\mu\nu} + \tfrac{1}{2}m_w^2 V^\mu V_\mu \\ & - g_w\overline{\psi}_i\gamma^\mu\psi_i V_\mu - \tfrac{1}{4}\vec{B}^{\mu\nu}.\vec{B}_{\mu\nu} + \tfrac{1}{2}m_\rho^2\vec{R}^\mu.\vec{R}_\mu \\ & - g_\rho\overline{\psi}_i\gamma^\mu\vec{\tau}\psi_i.\vec{R}^\mu - \tfrac{1}{2}m_\delta^2\delta^2 + g_\delta\overline{\psi}_i\delta\vec{\tau}\psi_i, \end{aligned} \tag{1}$$

where the field for σ meson is denoted by σ, that for ω meson is denoted by V_μ, and those for the isovector ρ and δ mesons are denoted by $\vec{R}_\mu$ and δ, respectively. The ψ_i are the Dirac spinors for the nucleons. An isospin is denoted by τ. Here, g_σ, g_ω, g_ρ, and g_δ are the coupling constants for the σ, ω, ρ, and δ mesons, respectively. M, m_σ, m_ω, m_ρ, and m_δ are the masses of the nucleons and σ, ω, ρ, and δ mesons, respectively. $\Omega^{\mu\nu}$ and $\vec{B}_{\mu\nu}$ are the field tensors for V^μ and $\vec{R}_\mu$, respectively. In this Langrangian, the contribution of the π meson has not been taken into account because, at the mean-field level, its contribution is zero due to its pseudoscalar nature [4,12].

From the relativistic Lagrangian, we obtain the field equations for the nucleons and mesons. The set of coupled equations is solved numerically by a self-consistent iteration method using the linear Horowitz and Serot (LHS) parameter set [3]. The root-mean-square (rms) matter radius is defined as

$$\langle r_m{}^2\rangle = \frac{1}{A}\int \rho(r) r^2 d\tau, \tag{2}$$

where A is the mass number and $\rho(r)$ is the spherical density.

Using the PCM [9,10], we deduce empirically the α preformation probability $P_0{}^{\alpha(\mathrm{emp})}$ from experimental data on a few α decays in the trans-lead region, using the HS-parameter-set-based spherical RMFT-HS densities. It is relevant to mention here that the mass and charge densities calculated by using RMFT [13] support the clustering effects in various heavy parents with observed cluster decays. In the PCM, the decay constant λ or half-life time $T_{1/2}$ is defined as [9,10,14]

$$\lambda_{\mathrm{PCM}} = \frac{\ln 2}{T_{1/2}} = \nu_0 P_0 P, \tag{3}$$

with the assault frequency $\nu_0 \sim 10^{21}$ s^{-1} for all of the cluster decays [10]. An empirical estimate of the preformation factor P_0 can be obtained as [14]

$$P_0{}^{\alpha(\mathrm{emp})} = \frac{\lambda_{\mathrm{expt}}}{\nu_0 P} \tag{4}$$

from the experimental λ_{expt} values [10] and calculated $\nu_0 P$. In the following, the values of $P_0{}^{\alpha(\mathrm{emp})}$ deduced by using the R3Y and M3Y NN interactions are compared. The other details of the methodology followed are given in Ref. [14].

The Wong formula [11] for fusion cross sections (σ_{fus}), at energies near the barrier within the context of the BPM, is given as

$$\sigma_{\mathrm{fus}}(E_{\mathrm{c.m.}}) = \frac{R_h{}^2\hbar\omega}{2E_{\mathrm{c.m.}}}\ln\left[1+\exp\left(\frac{2\pi}{\hbar\omega}(E_{\mathrm{c.m.}}-V_h)\right)\right], \tag{5}$$

where $\hbar\omega$ is the curvature of the inverted parabola and R_h and V_h are the barrier position and barrier height, respectively. $E_{\mathrm{c.m.}}$ is the center-of-mass energy for the target-projectile system. These quantities are taken from the total interaction potential between the projectile-target nuclei.

Moreover, the fusion barrier distribution $D(E_{\mathrm{c.m.}})$ $[d^2(E_{\mathrm{c.m.fus}})/dE_{\mathrm{c.m.}}]$ is calculated using the point difference formula

$$D(E) = [(E-\Delta E)\sigma_- - 2E\sigma + (E+\Delta E)\sigma_+]/(\Delta E)^2, \tag{6}$$

where σ_-, σ, and σ_+ indicate σ_{fus} at center-of-mass energies $E-\Delta E$, E, and $E+\Delta E$, respectively, with energy step size ΔE.

The nucleus-nucleus potentials between the nuclei in the DFM [1] are

$$V_n(\vec{R}) = \int \rho_1(\vec{r}_1)\rho_2(\vec{r}_2)v(|\vec{r}_1-\vec{r}_2+\vec{R}|\equiv r)d^3r_1 d^3r_2. \tag{7}$$

An effective NN interaction, like the phenomenological M3Y, is given as

$$v_{\mathrm{M3Y}}(r) = 7999\frac{e^{-4r}}{4r} - 2134\frac{e^{-2.5r}}{2.5r}, \tag{8}$$

where ranges are in femtometers and the strength is in million electron volts, plus a zero-range pseudopotential ($[J_{00}(E)\delta(r)$, EX], folded over the matter densities of the nuclei (ρ_1, ρ_2).

A microscopic NN interaction (R3Y) [2] from the linear RMFT-HS [3–6] Lagrangian, rather than a simple phenomenological prescription, was obtained as

$$v_{\mathrm{R3Y}}(r) = 11\,956\frac{e^{-3.97r}}{4r} + 4099\frac{e^{-3.90r}}{4r} - 6882\frac{e^{-2.64r}}{4r}. \tag{9}$$

We also successfully demonstrated its application [2] to various nuclear systems for evaluating some of the physical observables in the phenomenon of exotic CR by folding it with the RMFT densities of cluster and daughter nuclei to obtain the nucleus-nucleus potential. Adding Coulomb potential $V_C(R)$ $(=Z_1Z_2e^2/R)$ results in the nucleus-nucleus interaction potential $V(R)$ $[=V_n(R)+V_C(R)]$, used for calculating the Wentzel-Kramers-Brillouin (WKB) penetrability P, representing relative motion R, for α-decay studies and for calculating the V_h, R_h, and $\hbar\omega$ in the low-energy fusion reaction studies.

III. RESULTS AND DISCUSSIONS

Figure 1(a) illustrates the total interaction potentials $V(R)$ for α decay of ^{222}Ra, obtained for both the M3Y + EX and the R3Y + EX NN interactions using RMFT-HS densities. The penetration path with an energy equal to the Q value of decay also is shown here. Note that, compared to the M3Y NN interaction, the barrier is a bit higher for the R3Y case [shown more clearly in the inset of Fig. 1(b)], and hence P decreased by an order of magnitude, as is shown in Table I for some decays. Consequently, the deduced $P_0{}^{\alpha(\mathrm{emp})}$ (R3Y + EX) also are affected. However, in Table I, we find that the values of $P_0{}^{\alpha(\mathrm{emp})}$ (R3Y + EX) are similar to those of $P_0{}^{\alpha(\mathrm{emp})}$(M3Y + EX).

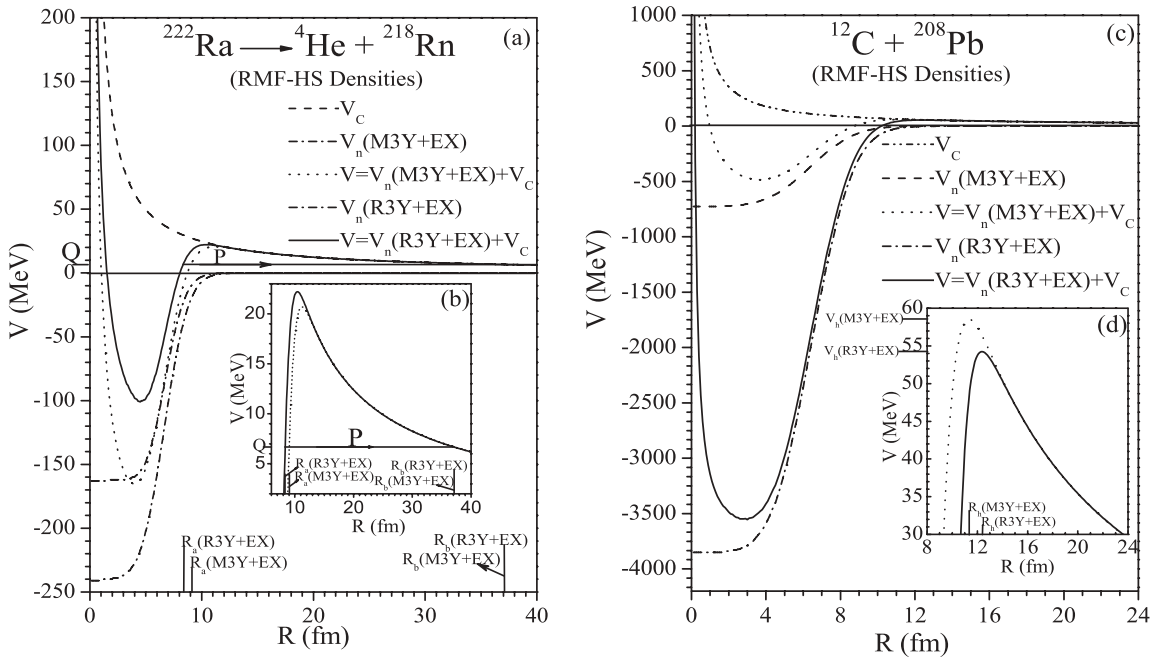

FIG. 1. (a) The total nucleus-nucleus optical potential $V(R)$ and the individual contributions [$V_n(R)$ (M3Y + EX) and $V_n(R)$ (R3Y + EX)] for the HS parameter set and the Coulomb potential $V_C(R)$ as a function of radial separation R for α decay of ^{222}Ra. (b) The inset of (a), same as (a) but with a changed scale in order to magnify the barrier. (c) Same as (a) but for the fusion reaction $^{12}C + ^{208}Pb$. (d) The inset of (c), same as (c) but with a changed scale in order to magnify the barrier height (V_h) and the position (R_h).

TABLE I. The WKB penetrability P, experimental decay constant $\lambda^{\alpha}_{\text{expt}}$, and the estimated $P_0{}^{\alpha(\text{emp})} = \lambda^{\alpha}_{\text{expt}}/\nu_0 P$ for α decays of various nuclei. The results are compared for the use of M3Y + EX and R3Y + EX NN interactions. The impinging frequency $\nu_0 \sim 10^{21}$ s^{-1} for each case. The Q values are calculated by using the experimental g.s. binding energies from Ref. [15].

Parent	Q (MeV)	P (M3Y + EX)	P ($R3Y + EX$)	$\lambda^{c}_{\text{expt}}$ (s^{-1})	$P_0{}^{\alpha(\text{emp})}$ (M3Y + EX)	$P_0{}^{\alpha(\text{emp})}$ (R3Y + EX)
^{221}Fr	6.457	2.954×10^{-22}	2.088×10^{-23}	2.406×10^{-02}	2.630×10^{-02}	3.721×10^{-01}
^{221}Ra	6.881	4.996×10^{-21}	3.517×10^{-22}	2.310×10^{-02}	1.445×10^{-03}	2.053×10^{-02}
^{222}Ra	6.679	8.567×10^{-22}	6.008×10^{-23}	1.824×10^{-02}	6.767×10^{-03}	9.649×10^{-02}
^{223}Ra	5.979	7.844×10^{-25}	5.407×10^{-26}	7.016×10^{-07}	3.010×10^{-04}	4.367×10^{-03}
^{224}Ra	5.789	9.740×10^{-26}	6.591×10^{-27}	2.189×10^{-06}	7.687×10^{-03}	1.136×10^{-01}
^{226}Ra	4.871	6.000×10^{-31}	3.929×10^{-32}	1.378×10^{-11}	8.606×10^{-03}	1.315×10^{-01}
^{223}Ac	6.783	8.186×10^{-22}	5.635×10^{-23}	5.440×10^{-03}	2.098×10^{-03}	3.048×10^{-02}
^{225}Ac	5.935	1.701×10^{-25}	1.142×10^{-26}	8.022×10^{-07}	1.598×10^{-03}	2.381×10^{-02}
^{226}Th	6.451	1.373×10^{-23}	9.262×10^{-25}	3.739×10^{-04}	8.858×10^{-03}	1.314×10^{-01}
^{228}Th	5.520	4.687×10^{-28}	2.732×10^{-29}	1.152×10^{-08}	8.677×10^{-03}	1.489×10^{-01}
^{230}Th	4.770	1.049×10^{-32}	6.638×10^{-34}	2.755×10^{-13}	1.002×10^{-02}	1.583×10^{-01}
^{230}U	5.993	1.316×10^{-26}	8.485×10^{-28}	3.857×10^{-07}	9.953×10^{-03}	1.544×10^{-01}
^{231}Pa	5.150	9.341×10^{-31}	5.909×10^{-32}	6.728×10^{-13}	2.646×10^{-04}	4.183×10^{-03}
^{232}U	5.414	1.103×10^{-29}	6.901×10^{-31}	3.074×10^{-10}	9.997×10^{-03}	1.598×10^{-01}
^{233}U	4.909	7.882×10^{-33}	4.860×10^{-34}	1.384×10^{-13}	6.627×10^{-03}	1.075×10^{-01}
^{234}U	4.858	3.817×10^{-33}	2.330×10^{-34}	9.011×10^{-14}	8.974×10^{-03}	1.470×10^{-01}
^{235}U	4.678	2.161×10^{-34}	1.328×10^{-35}	3.132×10^{-17}	5.624×10^{-05}	9.154×10^{-04}
^{236}U	4.573	3.829×10^{-35}	2.363×10^{-36}	9.142×10^{-16}	9.666×10^{-03}	1.566×10^{-01}
^{238}U	4.270	1.678×10^{-37}	1.036×10^{-38}	4.846×10^{-18}	1.179×10^{-02}	1.910×10^{-01}
^{237}Np	4.958	5.900×10^{-33}	3.639×10^{-34}	1.030×10^{-14}	6.598×10^{-04}	1.070×10^{-02}
^{236}Pu	5.867	4.142×10^{-28}	2.582×10^{-29}	7.730×10^{-09}	6.469×10^{-03}	1.038×10^{-01}
^{238}Pu	5.593	1.515×10^{-29}	1.051×10^{-30}	2.513×10^{-10}	5.908×10^{-03}	8.518×10^{-02}
^{241}Am	5.638	9.991×10^{-30}	6.124×10^{-31}	5.102×10^{-11}	1.819×10^{-03}	2.968×10^{-02}
^{242}Cm	6.216	3.733×10^{-27}	2.302×10^{-28}	4.195×10^{-08}	4.472×10^{-03}	7.251×10^{-02}

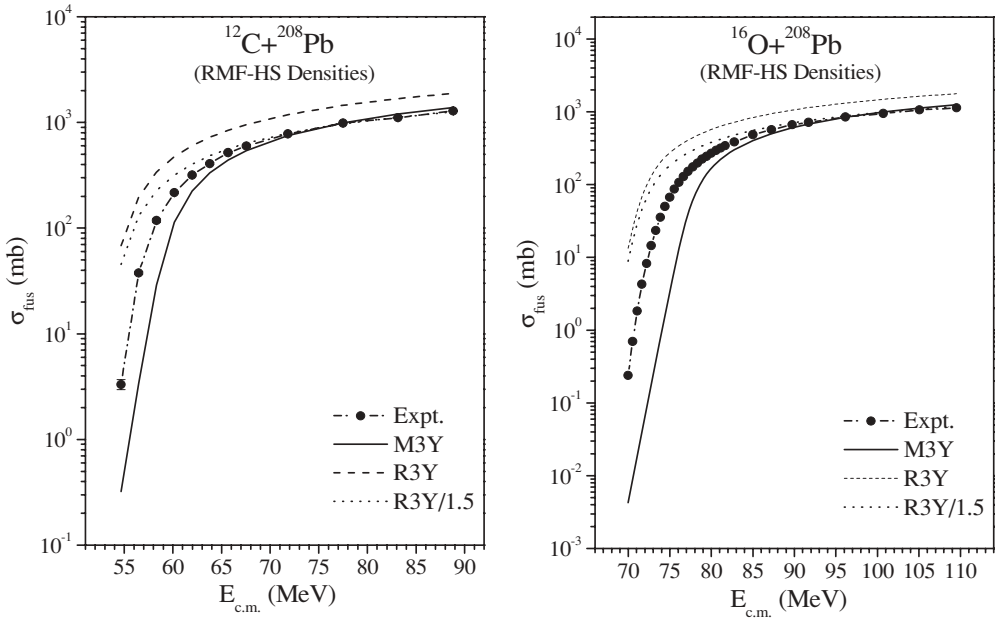

FIG. 2. (a) Variation of fusion cross section $\sigma_{\rm fus}$ as function of energy $E_{\rm c.m.}$ for the $^{12}C + ^{208}Pb$ system evaluated with the use of the M3Y and R3Y (solid and dashed lines, respectively) effective NN interactions, compared with the experimental data (shown by dash-dotted line and filled circles) obtained from Ref. [7]. The comparison also is shown for the $\sigma_{\rm fus}$ reduced by 1.5 times (dotted line) for the choice of the R3Y NN interaction. (b) Same as (a), but for $^{16}O + ^{208}Pb$. The experimental data for this reaction are taken from Ref. [8].

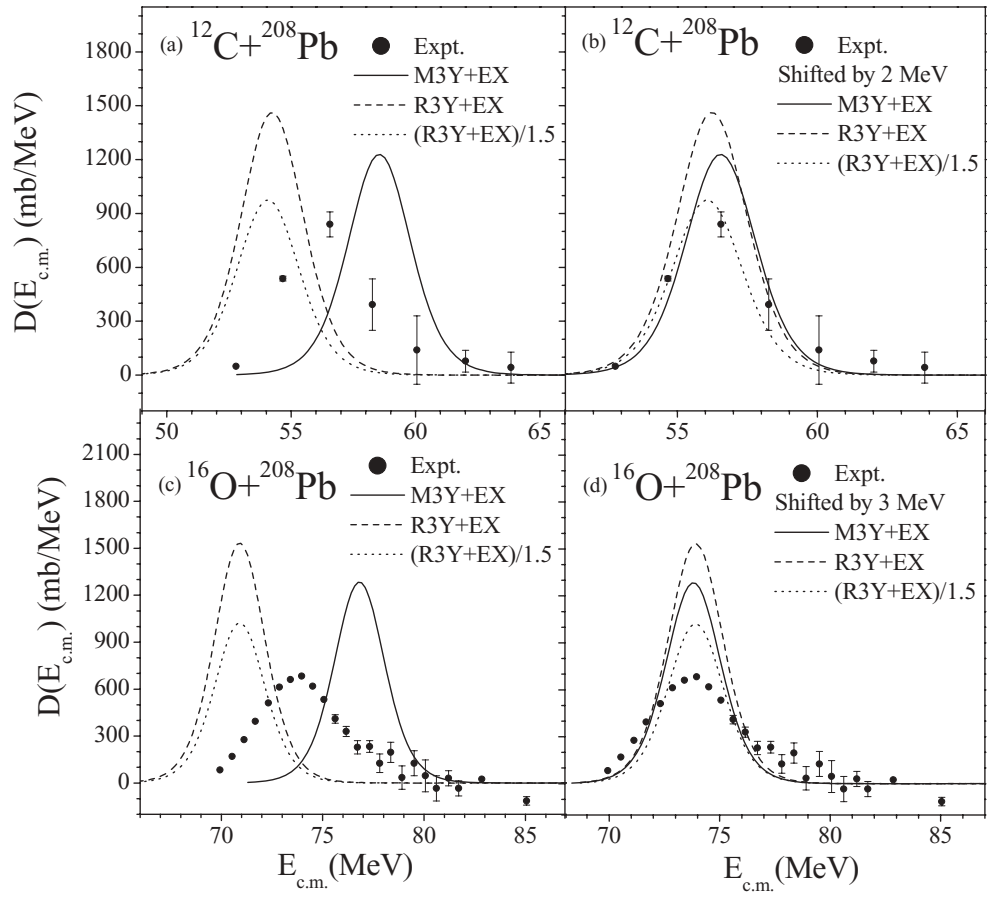

FIG. 3. Variation of the fusion barrier distribution $D(E_{\rm c.m.}) = d^2(E_{\rm c.m.}\sigma_{\rm fus})/dE^2_{\rm c.m.}$ as function of energy $E_{\rm c.m.}$ (a) and (b) for the $^{12}C + ^{208}Pb$ system corresponding to Fig. 2(a), compared with the experimental data (solid circles) obtained from Ref. [7]. Panels (c) and (d) are for the $^{16}O + ^{208}Pb$ system corresponding to Fig. 2(b), compared with the experimental data (solid circles) obtained from Ref. [8].

TABLE II. The quantities from the nucleus-nucleus interaction potential for the projectile-target systems $^{12}C + ^{208}Pb$ and $^{16}O + ^{208}Pb$, used in the calculations of σ_{fus} using Wong's formula, with the choice of the M3Y + EX and the R3Y + EX NN interactions, for RMF-HS densities. V_h, R_h, and $\hbar\omega$ represent height, radial position, and radius of curvature of the Coulomb barrier, respectively, for both the reactions.

Reaction	V_h (MeV)		R_h (fm)		$\hbar\omega$ (MeV)	
	(M3Y + EX)	(R3Y + EX)	(M3Y + EX)	(R3Y + EX)	(M3Y + EX)	(R3Y + EX)
$^{12}C + ^{208}Pb$	58.547	54.236	11.370	12.412	4.728	4.734
$^{16}O + ^{208}Pb$	76.813	70.911	11.544	12.651	4.652	4.685

Figure 1(c) illustrates the total interaction potentials $V(R)$ for the $^{12}C + ^{208}Pb$ system, obtained for both the M3Y + EX and the R3Y + EX NN interactions using the RMFT-HS densities. The modification of the barrier also is shown here for the two choices. Note that, compared to the M3Y NN interaction, the barrier height is lowered and the barrier position increased for the R3Y case [shown more clearly in the inset of Fig. 1(d)], and the related numbers are given in Table II including calculations for $\hbar\omega$. Consequently, the σ_{fus} calculations also are affected. Interestingly, in Figs. 2(a) and 2(b), we find that the variation of the fusion cross section σ_{fus} as a function of $E_{c.m.}$ for the $^{12}C + ^{208}Pb$ and $^{16}O + ^{208}Pb$ systems is quite similar for both the M3Y + EX and the R3Y + EX NN interactions in comparison with the experimental data [7,8], specifically when the calculated σ_{fus} is reduced by 1.5 times for the choice of the R3Y NN interaction. Moreover, in Fig. 3, we see that the $D(E_{c.m.})$ for both of the reactions $^{12}C + ^{208}Pb$ [Figs. 3(a) and 3(b)] and $^{16}O + ^{208}Pb$ [Figs. 3(c) and 3(d)] are similar for the M3Y + EX and R3Y + EX NN interactions in comparison with the experimental data [7,8].

In order to investigate the deviations from the experimental data for both of the choices (the M3Y + EX and R3Y + EX NN interactions), we also have calculated the fusion cross section using the formula in the framework of the direct reaction model [16,17], given as

$$\sigma_{fus} = \frac{\pi}{k^2}\sum_{\ell}(2\ell+1)\left(\sum_{j=1}^{n_{fus}} I_j^{(\ell)}\right). \tag{10}$$

Because the total potential is considered as a chain of n rectangular potentials, each one of which has an arbitrarily small width w, in the jth region, the strength and width of the potential are denoted by U_j and w_j, respectively, and $n_{fus} = \frac{R_{fus}}{w}$. For the jth segment, the corresponding absorption cross section is

$$\begin{aligned} I_j = \left(-\frac{1}{k_n}\right)\frac{\mathrm{Im}U_j}{|b_n|^2}\Bigg[&\frac{|b_j|^2}{2\mathrm{Im}k_j}e^{-2\mathrm{Im}k_j\, w_{j-1}}(e^{2\mathrm{Im}k_j\, w_j}-1) \\ &-\frac{|b_j|^2}{2\mathrm{Im}k_j}e^{2\mathrm{Im}k_j\, w_{j-1}}(e^{-2\mathrm{Im}k_j\, w_j}-1) \\ &+\frac{1}{\mathrm{Re}k_j}\mathrm{Im}(a_j b_j^* e^{2\mathrm{Im}k_j\, w_{j-1}}(e^{2i\mathrm{Re}k_j\, w_j}-1))\Bigg], \end{aligned} \tag{11}$$

and the wave number k_j is defined as $k_j = \sqrt{\frac{2m}{\hbar^2}(E - U_j)}$. The exact radius R_{fus} up to which the absorption cross section is to be calculated to explain the experimental σ_{fus} is known as the fusion radius. The value of the maximum angular momentum $\ell = R_{fus} \times \sqrt{\frac{2mE_{c.m.}}{\hbar^2}}$.

A similar procedure has been followed by one of us in an earlier study [17]. In Fig. 4(a), we still found a discrepancy for both of the choices. Although the calculated results are closer to the experimental data, the choice of the paramterized Wood-Saxon (WS) potential is able to fit the data very well. From Fig. 4(b), it is clear that the barrier (for $\ell = 0$) position and height play significant roles, which are different for both the M3Y + EX and the R3Y + EX NN interactions as well as the WS potential.

IV. SUMMARY AND CONCLUSIONS

Evidently, the effective NN interaction obtained from the RMFT Lagrangian, the R3Y, is applicable to study both

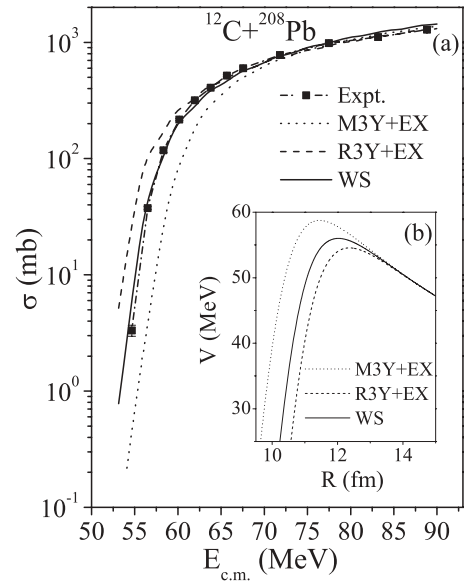

FIG. 4. (a) Variation of the fusion cross section σ_{fus} [calculated using Eq. (10)] as a function of energy $E_{c.m.}$ for the $^{12}C + ^{208}Pb$ system evaluated with the use of the M3Y and R3Y (dotted and dashed lines, respectively) effective NN interactions, compared with the experimental data (dash-dotted line and filled circles) obtained from Ref. [7] and with the calculations using the WS potential (solid line). (b) The total nucleus-nucleus optical potential $V(R)$ (for $\ell = 0$) as a function of radial separation R for the M3Y and R3Y (dotted and dashed lines, respectively) effective NN interactions and the WS potential (solid line).

the g.s. α-decay and the low-energy fusion phenomena with satisfactory precision. However, the present study has been carried out by taking into consideration only the linear terms of the σ, ω, and ρ meson fields. Apparently, it is relevant as well as interesting to study the link between the RMFT phenomenology and the effective NN interaction with the further inclusion of the nonlinear terms of these fields.

Concluding, we have shown in this work that the effective NN interaction, here called R3Y, derived from the simple linear Walecka Lagragian, can be used to study the fusion phenomena in heavy ion collisions rather than using the simple phenomenological prescription, which is presented eloquently in terms of the well-known built-in RMFT parameters of σ, ω, and ρ meson fields, that is, their masses (m_σ, m_ω, m_ρ) and coupling constants (g_σ, g_ω, g_ρ).

[1] G. R. Satchler and W. G. Love, Phys. Rep. **55**, 183 (1979).
[2] B. B. Singh, M. Bhuyan, S. K. Patra, and R. K. Gupta, arXiv:1011.5732v2.
[3] C. J. Horowitz and B. D. Serot, Nucl. Phys. A **368**, 503 (1981).
[4] B. D. Serot and J. D. Walecka, Adv. Nucl. Phys. **16**, 1 (1986).
[5] P. G. Reinhard, Rep. Prog. Phys. **52**, 439 (1989).
[6] S. K. Patra and C. R. Praharaj, Phys. Rev. C **44**, 2552 (1991).
[7] A. Mukherjee, D. J. Hinde, M. Dasgupta, K. Hagino, J. O. Newton, and R. D. Butt, Phys. Rev. C **75**, 044608 (2007).
[8] C. R. Morton, A. C. Berriman, M. Dasgupta, D. J. Hinde, J. O. Newton, K. Hagino, and I. J. Thompson, Phys. Rev. C **60**, 044608 (1999).
[9] S. S. Malik and R. K. Gupta, Phys. Rev. C **39**, 1992 (1989).
[10] R. K. Gupta and W. Greiner, Int. J. Mod. Phys. E **3**, 335 (1994).
[11] C. Y. Wong, Phys. Rev. Lett. **31**, 766 (1973).
[12] R. Brockmann, Phys. Rev. C **18**, 1510 (1978).
[13] S. K. Patra, R. K. Gupta, B. K. Sharma, P. D. Stevenson, and W. Greiner, J. Phys. G: Nucl. Part. Phys. **34**, 2073 (2007).
[14] B. B. Singh, S. K. Patra, and R. K. Gupta, Phys. Rev. C **82**, 014607 (2010).
[15] G. Audi, A. H. Wapstra, and C. Thiboult, Nucl. Phys. A **729**, 337 (2003).
[16] T. Udagawa, B. T. Kim, and T. Tamura, Phys. Rev. C **32**, 124 (1985).
[17] B. Sahu, G. S. Mallick, B. B. Sahu, S. K. Agarwalla, and C. S. Shastry, Phys. Rev. C **77**, 024604 (2008).